Density functional theory investigation of carbon monoxide adsorption on the kaolinite (001) surface*

Jian Zhao(赵健)†, Man-Chao He(何满潮), Xiang-Xing Hu(胡祥星), and Wei Gao(高炜)

State Key Laboratory for Geomechanics and Deep Underground Engineering, China University of Mining and Technology, Beijing 100083, *China*

(Received 6 January 2017; revised manuscript received 22 March 2017; published online 6 June 2017)

Carbon monoxide (CO) is a gaseous pollutant with adverse effects on human health and the environment. Kaolinite is a natural mineral resource that can be used for different applications, including that it can also be used for retention of pollutant gases. The adsorption behavior of carbon monoxide molecules on the (001) surface of kaolinite was studied systematically by using density-functional theory and supercell models for a range coverage from 0.11 to 1.0 monolayers (ML). The CO adsorbed on the three-fold hollow, two-fold bridge, and one-fold top sites of the kaolinite(001) was tilted with respect to the surface. The strongest adsorbed site of carbon monoxide on the kaolinite (001) surface is the hollow site followed by the bridge and top site. The adsorption energy of CO decreased when increasing the coverage, thus indicating the lower stability of surface adsorption due to the repulsion of neighboring CO molecules. In addition to the adsorption structures and energetics, the lattice relaxation, the electronic density of states, and the different charge distribution have been investigated for different surface coverages.

Keywords: kaolinite, adsorption, carbon monoxide, density functional theory

PACS: 91.60.–x, 68.43.Bc, 71.15.Nc **DOI:** 10.1088/1674-1056/26/7/079101

1. Introduction

High levels of gases such as pollutants coming from both natural and industrial activities are present in the atmosphere.[1,2] Carbon monoxide (CO) is categorized as a main pollutant by the US Environmental Protection Agency.[3] Carbon monoxide arises from the incomplete burning of materials, natural gas, industrial processes, sewage leaking, and biological decay.[4,5] Estimates of annual global emissions of CO vary from 2040 to 3315 terrogram (Tg).[6] The presence of CO in the atmosphere has a significant impact on climate, human health, and plants.[7–9] With the purpose of mitigating the effects it causes the health and longevity of both human beings and the earth's fragile ecosystems, many researchers have investigated experimentally the removal of CO using physical and chemical treatments.[10–13] Adsorption, as a technique with increasingly innovative applications, in number and type, is one of the most appropriate easy ways to remove CO gas pollutant before being liberated.[14–17]

Natural clay minerals, in particular, have received much attention as an abundant, possible low-cost, and environment friendly material that can be used for different applications. Because of their large propensity for adsorbing and immobilizing extraneous species, clay minerals can serve as material for pollution control, carriers of pesticides, liners in waste disposal, and barriers in nuclear waste management. Adsorption properties of clay minerals have been known for many years and used as adsorbent in the retention of CO taken from contaminated air. Numerous studies reported that clay minerals are used to remove CO.[1,18–20] For example, Venaruzzo's group investigated experimentally the adsorptions of CO, CO_2, and SO_2 gases on bentonitic clay minerals in natural state and after acid treatment. Itadani *et al.* have reported on low-pressure CO adsorption at room temperature on Al-pillared montmorillonite clay minerals by experimental techniques. Due to the limitations of experimental methods used, a theoretical analysis of the adsorption mechanism of CO molecules on natural clay minerals from a microscopic point of view will improve understanding of the adsorptive properties of the clay minerals–CO interface and the influence of CO adsorbed on the structure of clay minerals. Computer simulation in high-performance and the density-functional theory (DFT) offers accurate and inexpensive routes to study CO–solid interfaces at the molecular level, where the calculated results were very close to the experimental values.[21,22] Leydier's group calculated theoretically the adsorption of CO on amorphous silica-alumina (ASA) by using density functional theory, while the infrared features results matched closely the experimental data. Several works[23–25] have investigated the adsorption of carbon monoxide on Cu(I)-ZSM-5 or Ag(I)-ZSM-5 zeolite by using *ab initio* density functional theory study. These results are in accord with previous study and available experimental findings.

Kaolinite is a specific and very common clay mineral.[26,27] Existing experimental[28–30] and theoretical[31–36] data on the kaolinite $Al_2Si_2O_5(OH)_4$ surface are often rationalized by modelling two surfaces as an

*Project supported by the Young Elite Scientist Sponsorship Program by CAST and the National Natural Science Foundation of China (Grant No. 51574296).
†Corresponding author. E-mail: zhaojian0209@aliyun.com
© 2017 Chinese Physical Society and IOP Publishing Ltd

almost perfect 1:1 layer structure constituted by two different surfaces of aluminosilicate: one side of the lamella consists of a silica sheet in which Si atoms are coordinated tetrahedrally by oxygen anions and the other side consists of a gibbsite type sheet where aluminum atoms are coordinated octahedrally by oxygen anions and hydroxyl groups. Some studies showed that hydrogen bonding and a certain degree of van der Waals attraction exist between hydroxyl groups of Al oxide side and adjoining oxygen atoms of silica sheet in kaolinite.[37] Kaolinite microparticles exist as hexagonal plates with a dominant (001) basal surface with almost perfect cleavage; this is the plane mainly exposed in kaolinite crystals. The hydroxylated (001) surface of kaolinite is said to be hydrophilic and is the surface of primary interest in adsorption behavior studies.[37–39] Since we have tested the adsorption energy of carbon monoxide on siloxane and hydroxylated surface of kaolinite, respectively and the results showed that carbon monoxide adsorbs more weakly on siloxane surface than it does on the hydroxylated surface, here we only examine the hydroxylated (001) surface. Hence, a greater insight into the adsorption of CO molecules on hydroxylated (001) surface of kaolinite through a periodic density functional analysis is needed. In the present paper, the CO adsorption geometries, CO structure during and after being adsorbed, adsorption energies, the electronic density of states, charge transfer, and the electronic density of states were investigated systematically.

2. Methods

All total-energy calculations of adsorption behavior of CO on the kaolinite (001) were performed using VASP (Vienna *ab initio* simulation package) code[40] that allows the simulation of periodic systems within the DFT method. The electrons are fully quantum-mechanical treated by solving the Kohn–Sham equations. The local-density approximation (LDA) and the projector augmented wave potential of Blöchl are employed to describe the electron exchange-correlation energy as described below and the electron–ion interaction, respectively.[41–44] The energy cutoff for the plane-wave expansion was set to 400 eV, which was sufficient to ensure the error from calculations of adsorption energies below 0.01 eV. The so-called 'repeated slab' geometries were employed. The clean kaolinite (001) surface was modelled by a slab consisting of six atomic layers separated by 20 Å of vacuum. The CO molecules were adsorbed on the (001) surface of the slab in a symmetric way for all slab calculations. During the calculation, the positions of H, O, and Al atoms in the outermost three layers as well as the CO molecules were allowed to relax until the forces on the ions are below 0.02 eV/Å. The other atoms in the bottom three atomic layers of the slab were kept fixed at the calculated bulk positions.[45–47] Furthermore, a Fermi broadening of 0.02 eV was chosen to smear the occupation of the bands around E_F by a finite-T Fermi function and extrapolating to $T = 0$ K. Figure 1 shows the hydroxylated (001) surface of kaolinite after relaxation, in which 2/3 of the surface hydroxyl groups tilt and the other 1/3 hydroxyl groups are almost parallel to the surface. All calculations for adsorbed CO molecules in the twelve adsorption sites including three one-fold top sites (T_1–T_3), three two-fold bridge sites (B_1–B_3), and six three-fold hollow sites (H_1–H_6) have been performed with surface coverage region of $0 < \Theta \leq 1.0$.[49,50] To test the influence of supercell size on adsorption energy of carbon monoxide, we have calculated the adsorption energy of CO molecule on the kaolinite (001) slabs by using different models. The results imply that the difference of adsorption energy of CO on different models is very small and adsorption energy of CO molecule showed a trend of convergence with increasing the model size. The adsorption of CO molecules on the kaolinite (001) surface for 0.11 and 0.33 ML was calculated using the $p(3\times3)$ surface unit cell, but the $p(2\times2)$ surface unit cell for other (0.25, 0.5, 0.75, and 1.0 ML) coverages. Unless otherwise mentioned, we used Monkhorst–Pack[48] scheme with a $(3\times3\times1)$ k-point grid for the $p(2\times2)$ and $p(3\times3)$ surface cell. Based on the data of Hess and Saunders, the calculated lattice parameters of the bulk crystal structure of kaolinite were $a = 5.160$ Å, $b = 5.160$ Å, $c = 7.602$ Å, $\alpha = 81°$, $\beta = 89°$, and $\gamma = 60.18°$, and used in the present study.

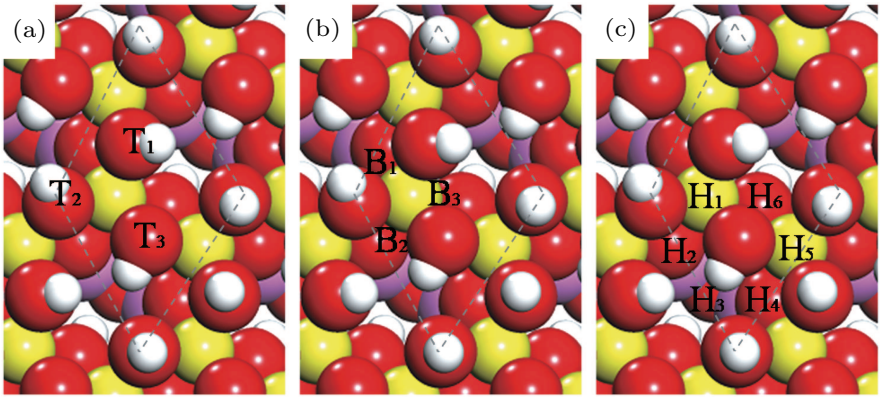


Fig. 1. (color online) Three adsorption sites including (a) top (T_1–T_3), (b) bridge (B_1–B_3), and (c) hollow (H_1–H_6) sites. Here, H atoms are shown by white spheres, while other O, Al, and Si atoms are shown by red spheres, yellow spheres, and purple spheres, respectively.

3. Results and discussion

In order to estimate the stability of these molecular adsorption configurations, the average adsorption energy of CO adsorption on the kaolinite (001) surface at different coverage is calculated by

$$E_{\rm ads}(\Theta) = -\frac{1}{N_{\rm CO}}[E_{\rm CO/kaolinite\ (001)} - E_{\rm kaolinite\ (001)} - N_{\rm CO}E_{\rm CO}]. \quad (1)$$

Here $N_{\rm CO}$ is the number of CO adsorbed. The $E_{\rm CO/kaolinite\ (001)}$ is the total energy for the kaolinite supercell plus $N_{\rm CO}$ CO molecules, depending on the coverage Θ (Θ is defined as the ratio of the number of molecules adsorbed to the number of hollow binding sites on the (001) surface). The $E_{\rm kaolinite\ (001)}$ is the total energy for the clean kaolinite surface and the $E_{\rm CO}$ is the free CO molecule total energy. A positive value of $E_{\rm ads}$ for CO molecules indicates the stable adsorption and a negative value indicates unstable reaction with respect to a free CO molecule. The adsorbed CO coverage was $0 < \Theta \leq 1.0$. Similar to Hu and Angelos and others, we have investigated all possible initial structures of the CO molecule adsorption. By employing the notation used in Fig. 1, the sites of Tops 1 to 3, Bridges 1 to 3, and Hollows 1 to 6 are represented. We considered two original molecular modes of parallel and vertical to the surface molecules with the carbon atom closer to the surface. After optimizing the adsorption model, the three adsorption states of the top, bridge, and hollow sites with tilted CO molecule became stable (Figs. 2(a)–2(c)). The C–O bond of adsorbed CO molecules on all 12 adsorption sites has an angle with the kaolinite (001) surface. The tilted orientation represents a configuration in which one carbon of CO forms a bond with the surface. Meanwhile, all three top and bridge and all six hollow adsorption sites for CO molecule have similar adsorption energy in the coverage region of $0 < \Theta \leq 1.0$, respectively. The calculated adsorption energies $E_{\rm ads}$ for these three kinds of surface sites with respect to the free molecule CO are shown in Table 1 at different coverages.

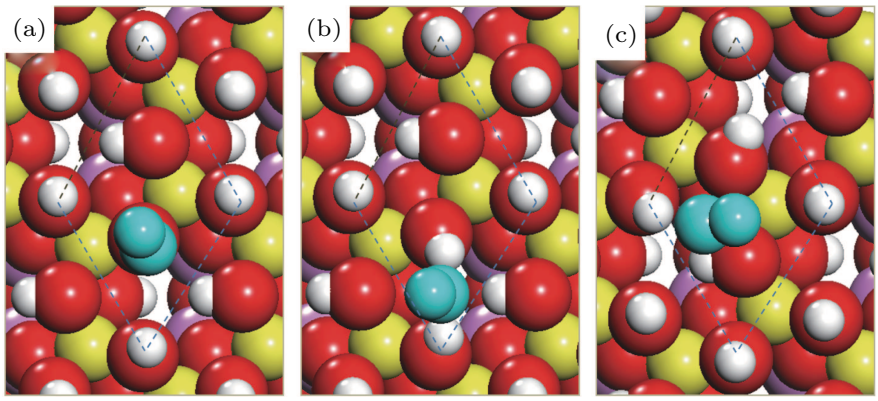


Fig. 2. (color online) Adsorption geometry of CO molecule on the (a) top, (b) bridge, and (c) hollow sites of kaolinite (001). The adsorbed CO molecule is shown in blue for clarity.

One can see that at the coverage of 0.11 ML (for $p(3\times3)$ structure), the adsorption configuration of tilted CO molecule on the hollow site was the most favorable compared with the other two sites. The next stable site for CO molecule is bridge and followed by the top sites. The adsorption energy of CO on hollow site of the kaolinite (001) surface was 0.37 eV and that for top and bridge sites were 0.20 and 0.17 eV lower, respectively. At the highest coverage of 1.0 ML (for $p(2\times2)$ structure), the hollow sites were preferred for inclined CO molecules adsorption, and the following stable adsorption sites were the bridge and the top sites. For the adsorption of CO molecules over kaolinite (001) surface, the calculated adsorption energies were 0.15, 0.22, and 0.29 eV at the top, bridge, and hollow sites, respectively. In the coverage regime of $0 < \Theta \leq 1.0$, the calculated adsorption energies of tilting CO (Table 1) revealed that the hollow site was more favorable than the bridge and the top sites at different coverages. Meanwhile, the quantities of the three adsorptions of top, bridge, and hollow display a modestly decreasing trend with the increase of CO, while the overall variation of the magnitude of $E_{\rm ads}$ was small. The decrease of adsorption with coverage indicates lower stability of surface adsorption.

Table 1. The adsorption energy $E_{\rm ads}$ (eV) for CO adsorbed on the kaolinite (001) surface at different coverages.

Site	ML0.11	ML0.25	ML0.33	ML0.5	ML0.75	ML1.0
Top	0.20	0.21	0.18	0.18	0.17	0.15
Bridge	0.27	0.27	0.26	0.25	0.23	0.22
Hollow	0.37	0.35	0.36	0.32	0.31	0.29

Calculated geometries for CO molecule adsorption on the top, bridge, and hollow sites of kaolinite (001) at $\Theta = 0.11$, 0.25, 0.33, 0.5, 0.75, and 1.0, including the C–O bond lengths $d_{\rm C-O}$ (Å) and the height of adsorbate CO above the surface as well as the topmost interlayer relaxation Δd_{12} are summarized in Table 2. The Δd_{12} value was calculated according to the equation $\Delta d_{12} = \frac{(d_{12}-d_0)}{d_0}$, where d_{12} is the distance between the first and second layers of the relaxed surface plane and d_0 is the interplanar spacing along the (001) direction of

bulk kaolinite. One can clearly see that the C–O bond lengths d_{C-O} vary little around 1.14 Å (in the gas phase) with increasing Θ values for all the adsorption sites. With respect to the height of adsorbate CO above the (001) surface, the results in Table 2 show that, for hollow adsorption site, the value was slightly shorter than the other two sites at the same coverage. A short height implied a strong interaction between CO and kaolinite surfaces. The above results imply that the hollow sites are the most stable. Note that for all three types of adsorption sites, the values of h_{C-O} increase with increasing CO coverages, which implies that the stability of adsorbed CO is reduced with increasing coverage.

Table 2. The calculated geometries for the CO molecule adsorption on top, bridge, and hollow sites of kaolinite (001). The C–O bond lengths d_{C-O} in Å of CO molecules were listed. The calculated adsorbate height (h_{C-O}) and the interlayer relaxation (Δd_{12}) for different coverage of atomic CO adsorption on kaolinite (001) surface.

Coverage Θ	d_{C-O}/Å			h_{C-O}/Å			Δd_{12}/%		
	top	bridge	hollow	top	bridge	hollow	top	bridge	hollow
0.25 ML	1.14	1.13	1.13	2.31	1.59	1.54	5.25	8.32	10.14
0.5 ML	1.13	1.14	1.14	2.41	1.81	1.79	9.38	9.27	11.63
0.75 ML	1.13	1.14	1.13	2.41	1.85	1.82	11.22	12.75	13.31
1.0 ML	1.13	1.14	1.14	2.48	2.03	1.92	12.89	14.17	17.74

Finally, we can easily see from Table 2 that the adsorption of CO on kaolinite (001) induces notable changes in the distance between the first and second layers of the substrate. In particular, for the three types of adsorptions, the value of Δd_{12} was positive from 5.25% to 12.89%, 8.32% to 14.17%, and 10.14% to 17.74% in the coverage regime of $0 < \Theta \leq 1.0$, respectively, which means that the distance between the topmost two atomic layers of the kaolinite (001) surface has expanded with increasing CO coverage. These changes reflected the strong influence of the CO adsorbates on the neighboring H and O atoms, thus, resulting from significant redistribution of the electronic structure. The results verified that the CO adsorption caused the outmost kaolinite (001) layer separation to relax back to something close to its 'ideal' bulk value.

To gain more insights into the bonding interaction of the chemisorbed CO molecule with the neighboring O atoms of the kaolinite (001) surface, we calculated and analyzed the electronic partial density of state (PDOS) and the electron density difference $\Delta\rho(r)$ for the adsorption system. The $\Delta\rho(r)$ was obtained by subtracting the electron densities of non-interacting component systems, $\rho_{\text{kaolinite (001)}}(r)+\rho_{CO}(r)$, from the density $\rho(r)$ of the CO/kaolinite (001) system, while retaining the atomic positions of the component system at the same location as in CO/kaolinite (001). A positive value (blue areas) of $\Delta\rho(r)$ for adsorption system indicates charge accumulation, while a negative value (yellow areas) corresponds to charge depletion upon binding. The isosurface value of the electron density difference is set at ± 0.003 e/Å^3 for all adsorption structures.

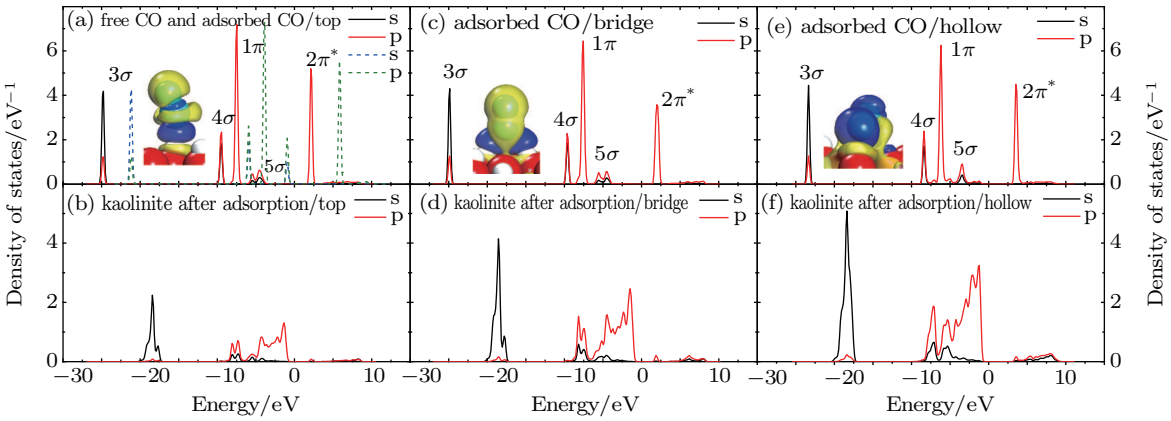


Fig. 3. (color online) Orbital-resolved partial DOS plots for the CO molecule and the surface O and H atoms (top, bridge, and hollow) with the coverage $\Theta = 0.25$: (a), (b) free (dashed line) and adsorbed CO (solid line), and adsorbed kaolinite (001) surface at the top adsorption site; (c), (d) adsorbed CO and adsorbed kaolinite (001) surface at the bridge adsorption site; (e), (f) adsorbed CO and adsorbed kaolinite (001) surface at the hollow adsorption site. The insets show the side view of electron density difference for the CO atoms at the (a) top, (c) bridge, and (e) hollow adsorption sites.

As a typical example, the PDOS of the adsorbed CO molecular orbitals (3σ, 4σ, 5σ, 1π, and $2\pi^*$) and the substrate H and O atoms coordinated with CO on the three stable adsorption configurations of the top, bridge, and hollow sites were plotted (Fig. 3); the electron-density differences are shown in Figs. 3(a), 3(c), and 3(e) (insets). The Fermi energy has been set at zero. The PDOS of the CO molecule in free state were also calculated for comparison in dashed line. After CO molecule adsorption on the top site of the (001) surface, the 3σ, 4σ, 1π, 5σ bonding, and 2π antibonding orbitals

of CO shifted down in energy by 3.65, 3.52, 3.66, 3.58, and 3.71 eV, respectively. The amplitudes of all bonding and antibonding orbitals are weaker than those in the free CO. Furthermore, the 5σ orbitals of adsorbed CO almost disappeared, indicating that electrons of CO transferred to neighboring H and O atom of kaolinite (001) surface. Correspondingly, the result is substantiated by the electron density difference as shown in the inset of Fig. 3(a). A large charge accumulation area exists between the C atom of adsorbate and neighboring H atoms of substrate.

The projected DOS for CO molecule (in the stable bridge) and the neighboring O and H atoms of the (001) surface are calculated (Figs. 3(c) and 3(d)). After adsorption, the bonding and antibonding orbitals of the CO molecule shift to lower energies and the amplitudes of 1π and 2π orbitals are weaker than those of free CO and the adsorbed CO on the top site. One can see a remarkable charge accumulation near the C atoms from the 3D electron-density difference (inset of Fig. 3(c)), indicating the 5σ bonding orbitals of CO molecule accepting electrons from the sp electronic states of H and O atoms. Meanwhile, electrons flow from H s state into C sp state. These results illustrate that the bridge site is more stable than the top site for CO molecule adsorption.

Finally, the PDOS of the tilted CO adsorbed on hollow site is depicted in Fig. 3(e), one new peak at -3.47 eV was observed in PDOS, which shows that the new peak was contributed by the 5σ hybridization with kaolinite s and p orbitals. The significant overlap emerged between adsorbed CO molecule and on surface O and H atoms electrons in the energy region from -9.05 to -0.76 eV. Furthermore, the amplitudes of all bonding and antibonding orbitals of adsorbed CO were obviously weaker than those in the free CO and the adsorbed CO on the other two types of adsorption sites. The 3σ, 4σ, 5σ, 1π, and 2π antibonding orbitals of the adsorbed CO molecule are observed to shift down to the lowest energies compared with the adsorbed CO on the top and the bridge sites. Meanwhile, the 3D electron density difference distribution of CO adsorbed on the hollow site is calculated, as shown in Fig. 3(e) (inset) for further understanding the electronic hybridization behavior. Upon CO adsorption, there is a remarkable charge depletion area between the C and on surface H atoms, while a manifested charge accumulation area was observed around C and O atoms of CO. The results indicate that more electrons of sp states of surface H and O atoms were transferred out and correspondingly the sp electronic state of C and O atoms of adsorbate accepting more electrons comparing with the top and bridge adsorption.

The PDOS for the CO molecule adsorption on top site and on surface H and O atoms at coverage of $\Theta = 0.25$ and $\Theta = 1.0$ ML, are shown in Figs. 4(a) and 4(b), respectively. At a high coverage ($\Theta = 1.0$), the narrow, low-amplitude peak at 4.12 eV was denoted as the 'CO p state' (Fig. 4(b)), which was mainly hybridized with the sp state of the neighboring H and O atoms; the hybridization between CO p and O sp states was negligible. At a low coverage ($\Theta = 0.25$), three prominent changes of PDOS for adsorbed CO and the neighboring O and H atoms occur: (i) the peaks in the CO 3σ, 4σ, 1π, 5σ bonding, and 2π antibonding shift down in energy; the amplitudes of all bonding and antibonding orbitals were much weaker than those in the coverage of $\Theta = 1.0$ ML; (ii) compared to the case where $\Theta = 1.0$ ML, the hybridization of CO p and surface O sp states was distinctly enhanced at the coverage of $\Theta = 0.25$ ML. The change in the CO p PDOS was due to the fact that the CO adatom was highly coordinated in low coverage of $\Theta = 0.25$ ML. In particular, the main peak around $E = -4.59$ eV in the CO p PDOS in Fig. 4(b) is a result of the hybridization between CO p states and O sp states; (iii) the new CO peak at -5.52 eV observed in Fig. 4(a) shows that the peak is contributed by the 5σ hybridization with kaolinite s and p orbitals. The results reveal that the 5σ orbital hybridizes with kaolinite sp orbitals strongly.

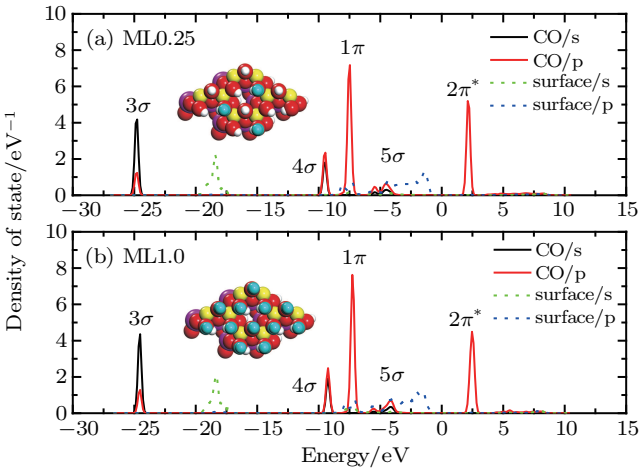


Fig. 4. (color online) The PDOS for the CO molecule adsorption on top site and the neighboring H and O atoms on surface at (a) $\Theta = 0.25$ and (b) $\Theta = 1.0$ ML, respectively.

4. Summary

The adsorption mechanism of CO molecule on the (001) surface of kaolinite are investigated systematically using first-principles DFT theory with total energy calculations. We consider a large range of coverage from 0.11 to 1.0 ML using two types of surface models (i.e., $p(3\times3)$ and $p(2\times2)$ surface unit cells) for adsorption on top, bridge, and hollow sites. The most stable among all possible pure adsorbed sites was the hollow site and followed by the bridge and top sites in the coverage range of $0 < \Theta \leq 1.0$. The atomic geometry, the lattice relaxation, the electronic density of states, and the charge density distribution after the CO molecule is adsorbed are also studied. The results show consistently the fundamental influence of hybridization and electron transfer between the CO molecule and surface H and O atoms. For the top site adsorption, the 3D distribution of electron density difference was the least, while the distribution of electron density difference is the most in case

of hollow sites adsorption. The d_{C-O} length of all adsorption sites varies little around 1.14 Å with increasing Θ values. Remarkably, this influence on the energy decreases with increasing CO coverage. These conclusions are in accord with available experimental findings. The great variety of physical and chemical treatments may be used for removal of CO with clay minerals, even modified clay minerals, in future. It is expected that our theoretical results would provide useful information for the development of CO removal, particularly in terms of protecting our environment.

References

[1] Venaruzzo J L, Volzone C, Rueda M L and Ortida J 2002 *Microporous Mesoporous Mater.* **56** 73
[2] Mahdi R S and Sahar Y 2015 *Comput. Condens. Matter* **3** 21
[3] Jin Y M, Guo L, Veiga M C and Kennes C 2009 *Chemosphere* **74** 332
[4] Huang X Y, Wang Y, Xing Z Y and Du K 2016 *Sci. Total Environ.* **565** 697
[5] Donateo T, Licci F, D'Elia A, Colangelo G, Laforgia D and Ciancarelli F 2015 *Appl. Energ.* **157** 675
[6] Tilley D R and Mentzer J 2006 *J. Air Waste Manage.* **56** 115
[7] Peng L, Zhao C, Lin Y, Zheng X, Tie X and Chan L 2007 *Chemosphere* **66** 1383
[8] Omaye S T 2002 *Toxicology* **180** 139
[9] Levy R J 2015 *Neurotoxicol. Teratol.* **49** 31
[10] Jo J O, Trinh H Q, Kim S H and Mok Y S 2016 *Chem. Eng. J.* **299** 93
[11] Shen Y S, Zong Y H, Ma Y F, Zhu S M and Jin Q J 2016 *Fuel* **180** 727
[12] Sushil S and Batra V S 2012 *J. Hazard. Mater.* **203** 264
[13] Makeey A G, Peskoy N V and Yanagihara H 2012 *Appl. Catalysis B: Environ.* **119** 273
[14] Rahimpour M R, Mazinani S, Vaferi B and Baktash M S 2011 *Appl. Energ.* **88** 41
[15] Sawicki J A, Marcinkowska K and Wagner F E 2010 *Nucl. Instrum. Meth. B* **268** 2544
[16] Hörtz P, Ruff P and Schäfer R 2015 *Surf. Sci.* **639** 66
[17] Ayastuy J L, Fernández-Puertas E, González-Marcos M P and Gutiérrez-Ortiz M A 2012 *Int. J. Hydrogen Energ.* **37** 7385
[18] Itadania A, Tanaka M, Abe T, Taguchi H and Nagao M 2007 *J. Colloid Interf. Sci.* **313** 747
[19] Brunauer S, Emmett P H and Teller E 1938 *J. Am. Chem. Soc.* **60** 309
[20] Leydier F, Chizallet C, Costa D and Raybaud P 2012 *Chem. Commun.* **48** 4076
[21] Zhao X J, Zhang R G, Ling L X and Wang B J 2014 *Appl. Surf. Sci.* **320** 681
[22] Bechthold P, Ardhengi J S, Juan A, González E A and Jasen P V 2014 *Appl. Surf. Sci.* **315** 467
[23] Zheng X B, Zhang Y H and Bell A T 2007 *Phys. Chem. C* **111** 13442
[24] Kuroda Y, Kumashiro R and Nagao M 2002 *Appl. Surf. Sci.* **196** 408
[25] Qiu Z Z, Yu Y X and Mi J G 2012 *Appl. Surf. Sci.* **258** 9629
[26] Chen Y H and Lu D L 2015 *Appl. Surf. Sci.* **104** 221
[27] Brigatti M F, Galan E and Theng B K G 2006 *General Introduction: Clays, Clay Minerals, and Clay Science of Handbook of Clay Science* (Elsevier Ltd), pp. 27–30
[28] Adams J M 1983 *Clay. Clay. Miner.* **31** 352
[29] Benco L, Tunega D, Hafner J and Lischka H 2001 *Am. Miner.* **86** 1057
[30] Bish D L 1993 *Clay. Clay. Miner.* **41** 738
[31] Hayashi S 1997 *Clay. Clay. Miner.* **45** 724
[32] Hess A C and Saunders V R 1992 *J. Phys. Chem.* **11** 4367
[33] Hobbs J D, Cygan R T, Nagy K L, Schultz P A and Sears M P 1997 *Am. Miner.* **82** 657
[34] Plancon A, Giese R F Jr, Snyder R, Drits V A and Bookin A S 1989 *Clay. Clay. Miner.* **37** 195
[35] Teppen B J, Rasmussen K, Bertsch P M, Miller D M and Schäferll L 1997 *J. Phys. Chem.* **101** 1579
[36] Hu X L and Angelos M 2008 *Surf. Sci.* **602** 960
[37] Sato H, Ono K, Johnston C T and Yamagishi A 2005 *Am. Miner.* **90** 1824
[38] Šolc R, Gerzabek M H, Lischka H and Tunega D 2011 *Geoderma* **169** 47
[39] Giese R F J R 1973 *Clay. Clay. Miner.* **21** 145
[40] Kresse G and Furthmüller J 1996 *Phys. Rev. B* **54** 11169
[41] Blöchl P E 1994 *Phys. Rev. B* **50** 17953
[42] Sun B, Zhang P, Wang Z G, Duan S Q, Zhao X G, Ma X C and Xue Q K 2008 *Phys. Rev. B* **78** 1758
[43] Zhang X L, Wu Y Y, Shao X H, Lu Y and Zhang P 2016 *Chin. Phys. B* **25** 057102
[44] Hua N, Tao X M and Tan M Q 2012 *Chin. Phys. B* **21** 016802
[45] Yang Y, Zhou G, Wu J, Duan W H, Xue Q K, Gu B L, Jiang P, Ma X C and Zhang S B 2008 *J. Chem. Phys.* **128** 164705
[46] Hua N, Lan Z Q, Guo J and Tan M Q 2015 *Appl. Surf. Sci.* **328** 641
[47] Wang Y J, Wang C Y and Wang S Y 2011 *Chin. Phys. B* **20** 036801
[48] Monkhorst H J and Pack J D 1976 *Phys. Rev. B* **13** 5188
[49] Zhao J and He M C 2014 *Appl. Surf. Sci.* **317** 153
[50] He M C and Zhao J 2012 *Chin. Phys. Lett.* **29** 153